

Nonlinear aerodynamic stability analysis of orthotropic membrane structures with large amplitude

Zhoulian Zheng^{*1,2}, Yunping Xu¹, Changjiang Liu¹, Xiaoting He¹ and Weiju Song¹

¹College of Civil Engineering, Chongqing University, Chongqing 400045, P.R. China

²Key Laboratory of New Technology for Construction of China in Mountainous Area, Chongqing University, Chongqing 400045, P.R. China

(Received June 14, 2010, Accepted October 25, 2010)

Abstract. The aerodynamic stability of orthotropic tensioned membrane structures with rectangular plane is theoretically studied under the uniform ideal potential flow. The aerodynamic force acting on the membrane surface is determined by the potential flow theory in fluid mechanics and the thin airfoil theory in aerodynamics. Then, based on the large amplitude theory and the D'Alembert's principle, the interaction governing equation of wind-structure is established. Under the circumstances of single mode response, the Bubnov-Galerkin approximate method is applied to transform the complicated interaction equation into a system of second order nonlinear differential equation with constant coefficients. Through judging the stability of the system characteristic equation, the critical divergence instability wind velocity is determined. Finally, from different parametric analysis, we can conclude that it has positive significance to consider the characteristics of orthotropic and large amplitude for preventing the instability destruction of structures.

Keywords: membrane structures; orthotropic; large amplitude; wind-structure interaction; critical instability wind velocity.

1. Introduction

Because of the membrane structure's economy, beauty, and less dead weight, it is widely applied to large span structures, such as large-scale stadium, exhibition center, works of decoration, and so on. But for its less dead weight, low local stiffness and low natural frequency, the kind of structure is very sensitive to the wind loads. As the wind velocity reaches a certain value, the aerodynamic instability phenomenon may occur. In the wind tunnel tests for suspended cable roof models, Miyake *et al.* (1992) and Kawakita *et al.* (1992) have observed this kind of aerodynamic instability phenomenon. In actual engineering, the membrane roofs of the Cheju World Cup stadium in Korea and Wenzhou University stadium in China have the experience of failure with local or total destruction under the wind loads less than the design value. It has caused the scholars great attention to study the aerodynamic stability of this kind of structure under wind loads.

At present, the results of qualitative analysis are more consistent about the mechanism of aerodynamic instability in membrane structure (Minarni *et al.* 1993, Bingnan *et al.* 2003): At the lower wind velocity, this kind of structure vibrates mainly in single mode for the divergence

*Corresponding author, Ph.D., E-mail: zhengzhoulian@yahoo.com.cn

instability; with the speed increasing, it presents multi-mode coupling state for the flutter instability. However, studies on quantitative analysis are not enough. Sygulski (1994, 1997) applied the FEM (Finite element method) & BEM (Boundary element method) to derive the critical instability wind velocity of a piece of membrane supported on the rigid board in the uniform potential flow. Attar *et al.* (2005) used a reduced order system identifying approach to analysis the nonlinear structural behavior of aeroelastic configurations and the results compare well with those from a high-fidelity aeroelastic model. Stanford *et al.* (2007, 2008) invented a novel experimental setup which integrated a wind tunnel with a visual image correlation system for simultaneous measurement of wing displacements, strains, and aerodynamic loads, and demonstrated that the numerical and experimental data are suitable correspondence for moderate angles of attack. Scott *et al.* (2007) established the NASTRAN normal modes and the finite difference membrane model with 3rd order piston theories to simulate the dynamic aeroelastic stability of membrane structures for aero-capture, and the results obtained are compared with the static aeroelastic analysis. Yang *et al.* (2006) derived the critical wind velocity by determining the stability of the wind-roof interaction equation, Li *et al.* (2006) did it through judging the frequency characteristic of the system characteristic equation.

In this paper we take the tow characteristics of orthotropic and geometric nonlinearity in actual membrane structure into consideration and theoretically study the aerodynamic stability of rectangular orthotropic membrane structure. Based on the large amplitude theory and D'Alembert's principle, the governing equation is addressed in Section 2. Applying the Bubnov-Galerkin approximate method, Section 3 is devoted to deduce the critical instability wind velocity. In Section 4 some computational examples are given to analyze the influence of each parameter. And some conclusions are obtained in Section 5.

2. Governing equations

2.1 Structure model

The membrane structure studied with rectangular plane is orthotropic. Its two orthogonal directions are the two principal fiber directions, and the material characteristics of the two principal fiber directions are different. Assume that it is clamped on four edges. The two principal fiber directions are x and y . a and b denote the spans in x and y , respectively; N_{0x} and N_{0y} denote initial tension in x and y , respectively, as shown in Fig. 1.

2.2 Dynamic governing equations and boundary conditions

According to the large amplitude theory of membranes and D'Alembert's principle (Zheng *et al.* 2009), the dynamic governing partial differential equation and compatibility equation of orthotropic membrane are

$$\begin{cases} (N_x + N_{0x}) \frac{\partial^2 w}{\partial x^2} + (N_y + N_{0y}) \frac{\partial^2 w}{\partial y^2} - 2\rho_0 \xi_0 \frac{\partial w}{\partial t} + p_z = \rho_0 \frac{\partial^2 w}{\partial t^2} \\ \frac{1}{E_1 h} \frac{\partial^2 N_x}{\partial y^2} - \frac{\mu_2}{E_2 h} \frac{\partial^2 N_y}{\partial y^2} - \frac{\mu_1}{E_1 h} \frac{\partial^2 N_x}{\partial x^2} + \frac{1}{E_2 h} \frac{\partial^2 N_y}{\partial x^2} - \frac{1}{Gh} \frac{\partial^2 N_{xy}}{\partial x \partial y} = \left(\frac{\partial^2 w}{\partial x \partial y} \right)^2 - \frac{\partial^2 w}{\partial x^2} \frac{\partial^2 w}{\partial y^2} \end{cases} \quad (1)$$

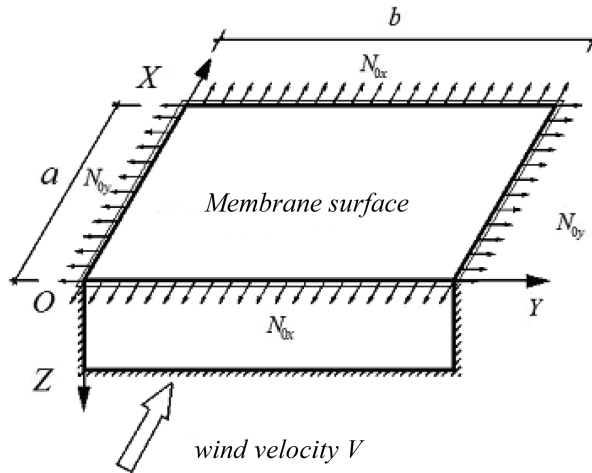


Fig. 1 Rectangular plane membrane structure with four edges clamped

where ρ_0 denotes the area density of membrane; N_x and N_y the additional tension in x and y , respectively; N_{0x} and N_{0y} the initial tension in x and y , respectively; N_{xy} the shear force; w the deflection: $w(x, y, t)$; h the membrane's thickness; E_1 and E_2 the Young's modulus in x and y , respectively; G the shear modulus; μ_1 and μ_2 the Poisson's ratio in x and y , respectively; ξ_0 the structure-self's damping coefficient; p_z the external loads in z : $p_z(t)$.

While the membrane is in vibration, the effect of shearing stress is so small that we may take $N_{xy} = 0$. Introducing the stress function $\varphi(x, y, t)$ and letting $N_x = h(\partial^2 \varphi / \partial y^2)$, $N_y = h(\partial^2 \varphi / \partial x^2)$, $N_{xy} = -h(\partial^2 \varphi / \partial x \partial y) = 0$, $\partial^2 N_x / \partial^2 x = \partial^2 N_y / \partial^2 y = h(\partial^4 \varphi / \partial x^2 \partial y^2) = -\partial^2 N_{xy} / \partial x \partial y = 0$, Eq. (1) can be simplified as follows

$$\left(h \frac{\partial^2 \varphi}{\partial y^2} + N_{0x} \right) \frac{\partial^2 w}{\partial x^2} + \left(h \frac{\partial^2 \varphi}{\partial x^2} + N_{0y} \right) \frac{\partial^2 w}{\partial y^2} - 2\rho_0 \xi_0 \frac{\partial w}{\partial t} + p_2 - p_1 = \rho_0 \frac{\partial^2 w}{\partial t^2} \quad (2)$$

$$\frac{1}{E_1} \frac{\partial^4 \varphi}{\partial y^4} + \frac{1}{E_2} \frac{\partial^4 \varphi}{\partial x^4} = \left(\frac{\partial^2 w}{\partial x \partial y} \right)^2 - \frac{\partial^2 w}{\partial x^2} \frac{\partial^2 w}{\partial y^2} \quad (3)$$

where φ is the stress function: $\varphi(x, y, t)$; p_1 and p_2 are the atmospheric pressure indoor and outdoor, respectively; and suppose that p_1 equals the static atmospheric pressure p_∞ .

The corresponding boundary conditions can be expressed as follows

$$\begin{cases} w(0, y, t) = 0 \\ w(a, y, t) = 0 \end{cases}, \begin{cases} w(x, 0, t) = 0 \\ w(x, b, t) = 0 \end{cases} \quad (4)$$

3. Critical instability wind velocity

3.1 The aerodynamic

Dowell (1970) pointed out that the air viscosity should be considered if the vibration wavelength is close to the air boundary layer thickness. But in types of civil engineering structures the low

order mode often plays a dominant role when vibrating, so the wavelength is far greater than the boundary layer thickness. Uematsu *et al.*'s (1986) experimental studies showed that the boundary layer turbulence has less effect on the structure's response under wind loads. So we ignore the tow factors in this paper and suppose that the potential flow is uniform and incompressible, velocity value V and direction along x .

According to the fluid Bernoulli Equation the outdoor dynamic pressure p_2 is (Forsching 1980)

$$p_2 = -\rho \left(V \frac{\partial \phi'}{\partial x} + \frac{\partial \phi'}{\partial t} \right)_{z=z_0} + p_\infty \quad (5)$$

where ρ is air density; z_0 the surface function under initial stress: $z_0(x, y)$; and ϕ' the velocity perturbation potential: $\phi'(x, y, z, t)$.

According to the potential theory, $\phi'(x, y, z, t)$ in Eq. (5) needs to satisfy the Laplace Eq. (6) and boundary conditions Eq. (7)

$$\frac{\partial^2 \phi'}{\partial x^2} + \frac{\partial^2 \phi'}{\partial y^2} + \frac{\partial^2 \phi'}{\partial z^2} = 0 \quad (6)$$

$$v_z = \frac{\partial \phi'}{\partial z} = V \frac{\partial z}{\partial x} + \frac{\partial z}{\partial t} \quad (7)$$

where v_z denotes the flow velocity component in z .

According to the thin airfoil theory in aerodynamics, $\phi'(x, y, z, t)$ satisfying Eq. (6) and Eq. (7) can be supposed as follows (Ivovich *et al.* 1991)

$$\phi'(x, y, z, t) = \frac{1}{2\pi} \iint_{Ra} \frac{\left(V \frac{\partial z}{\partial x} + \frac{\partial z}{\partial t} \right)_{x=\xi, y=\eta}}{\sqrt{(x-\xi)^2 + (y-\eta)^2 + z^2}} d\xi d\eta \quad (8)$$

where Ra denotes the structure's projection area in the plane xoy .

3.2 Critical wind velocity

Take the membrane surface function under wind loads as

$$z(x, y, t) = z_0(x, y) + w(x, y, t) \quad (9)$$

for the initial surface function $z_0(x, y) = 0$, then

$$z(x, y, t) = w(x, y, t) \quad (10)$$

Substituting Eq. (10) into Eq. (8), then substituting the result into Eq. (5) yields

$$p_2 = -\frac{\rho}{2\pi} \left[-V \iint_{Ra} \frac{\left(V \frac{\partial w}{\partial x} + \frac{\partial w}{\partial t} \right)_{x=\xi, y=\eta} (x-\xi)}{\left(\sqrt{(x-\xi)^2 + (y-\eta)^2} \right)^3} d\xi d\eta + \iint_{Ra} \frac{\left(V \frac{\partial^2 w}{\partial x \partial t} + \frac{\partial^2 w}{\partial t^2} \right)_{x=\xi, y=\eta}}{\sqrt{(x-\xi)^2 + (y-\eta)^2}} d\xi d\eta \right] + p_\infty \quad (11)$$

Letting:

$$r = \sqrt{(x - \xi)^2 + (y - \eta)^2}$$

$$A_1 = \frac{\rho + \rho^*}{2\pi} \iint_{Ra} \frac{1}{r} \left(\frac{\partial^2 w}{\partial t^2} \right)_{x=\xi, y=\eta} d\xi d\eta, \quad A_2 = \frac{\rho V}{2\pi} \iint_{Ra} \frac{1}{r} \left(\frac{\partial^2 w}{\partial x \partial t} \right)_{x=\xi, y=\eta} d\xi d\eta$$

$$A_3 = \frac{\rho V^2}{2\pi} \iint_{Ra} \frac{1}{r^3} \left(\frac{\partial w}{\partial x} \right)_{x=\xi, y=\eta} (x - \xi) d\xi d\eta, \quad A_4 = \frac{\rho V}{2\pi} \iint_{Ra} \frac{1}{r^3} \left(\frac{\partial w}{\partial t} \right)_{x=\xi, y=\eta} (x - \xi) d\xi d\eta$$

Eq. (11) can be simplified as

$$p_2 = -A_1 - A_2 + A_3 + A_4 + p_\infty \tag{12}$$

where the domain of integration Ra is $\{0 \leq \xi \leq a, 0 \leq \eta \leq b\}$; in A_1 the gas inertial load ρ^* attached to the lower surface is taken into consideration (Yang *et al.* 2006), assume $\rho^* = \rho$.

Substituting Eq. (12) into Eq. (2) yields

$$\left(h \frac{\partial^2 \varphi}{\partial y^2} + N_{0x} \right) \frac{\partial^2 w}{\partial x^2} + \left(h \frac{\partial^2 \varphi}{\partial x^2} + N_{0y} \right) \frac{\partial^2 w}{\partial y^2} - 2\rho_0 \xi_0 \frac{\partial w}{\partial t} = \rho_0 \frac{\partial^2 w}{\partial t^2} + A_1 + A_2 - A_3 - A_4 \tag{13}$$

Functions that satisfy the boundary conditions Eq. (4) are as follows

$$\begin{cases} w(x, y, t) = \sum_{i=1}^n T_i(t) W_i(x, y) \\ \varphi(x, y, t) = \sum_{i=1}^n \tilde{T}_i(t) \Phi_i(x, y) \end{cases} \tag{14}$$

where $W_i(x, y)$ is the given mode shape function; $\Phi_i(x, y), T_i(t)$ and $\tilde{T}_i(t)$ are the unknown functions.

As the flutter instability is multi-mode coupling instability, it's difficult to solve this kind of nonlinear equation. This paper investigates the divergence instability based on single mode vibration mode. Assume that the single mode shape function is

$$W(x, y) = \sin \frac{m\pi x}{a} \sin \frac{n\pi y}{b} \tag{15}$$

where m and n are integers and denote the orders of vibration mode in x and y , respectively. Eq. (15) satisfies the boundary conditions automatically.

So the displacement function is

$$w(x, y, t) = T(t) \sin \frac{m\pi x}{a} \sin \frac{n\pi y}{b} \tag{16}$$

Substituting Eq. (16) into Eq. (3) yields

$$\frac{1}{E_1} \frac{\partial^4 \varphi}{\partial y^4} + \frac{1}{E_2} \frac{\partial^4 \varphi}{\partial x^4} = \frac{m^2 n^2 \pi^4}{2a^2 b^2} T^2(t) \left(\cos \frac{2m\pi x}{a} + \cos \frac{2n\pi y}{b} \right) \tag{17}$$

Assume that the function which satisfied Eq. (17) is

$$\begin{cases} \varphi(x,y,t) = T^2(t)\Phi(x,y) \\ \Phi(x,y) = \alpha\cos\frac{2m\pi x}{a} + \beta\cos\frac{2n\pi y}{b} \end{cases} \tag{18}$$

Substituting Eq. (18) into Eq. (17) yields

$$\alpha = \frac{E_2 a^2 n^2}{32 b^2 m^2}, \quad \beta = \frac{E_1 b^2 m^2}{32 a^2 n^2}$$

Substituting Eq. (16) and Eq. (18) into Eq. (13) yields

$$\begin{aligned} \left(\rho_0 W + \frac{\rho}{\pi} \gamma_1\right) T''(t) + \left[\frac{\rho V}{2\pi}(\gamma_2 - \gamma_4) + 2\rho_0 \xi_0 W\right] T'(t) - \left(N_{0x} \frac{\partial^2 W}{\partial x^2} + N_{0y} \frac{\partial^2 W}{\partial y^2} + \frac{\rho V^2}{2\pi} \gamma_3\right) T(t) \\ - h \left(\frac{\partial^2 \Phi}{\partial y^2} \frac{\partial^2 W}{\partial x^2} + \frac{\partial^2 \Phi}{\partial x^2} \frac{\partial^2 W}{\partial y^2}\right) T^3(t) = 0 \end{aligned} \tag{19}$$

where

$$\begin{aligned} \gamma_1 &= \iint_{Ra}^1 \frac{1}{r} (W)_{x=\xi} d\xi d\eta = \iint_{Ra}^1 \sin \frac{m\pi\xi}{a} \sin \frac{n\pi\eta}{b} d\xi d\eta \\ \gamma_2 &= \iint_{Ra}^1 \frac{1}{r} \left(\frac{\partial W}{\partial x}\right)_{x=\xi} d\xi d\eta = \frac{m\pi}{a} \iint_{Ra}^1 \cos \frac{m\pi\xi}{a} \sin \frac{n\pi\eta}{b} d\xi d\eta \\ \gamma_3 &= \iint_{Ra}^1 \frac{1}{r^3} \left(\frac{\partial W}{\partial x}\right)_{x=\xi} (x-\xi) d\xi d\eta = \frac{m\pi}{a} \iint_{Ra}^1 \frac{1}{r^3} (x-\xi) \cos \frac{m\pi\xi}{a} \sin \frac{n\pi\eta}{b} d\xi d\eta \\ \gamma_4 &= \iint_{Ra}^1 \frac{1}{r^3} (W)_{x=\xi} (x-\xi) d\xi d\eta = \iint_{Ra}^1 \frac{1}{r^3} (x-\xi) \sin \frac{m\pi\xi}{a} \sin \frac{n\pi\eta}{b} d\xi d\eta \end{aligned}$$

According to the Bubnov-Galerkin method (Shin *et al.* 2004), Eq. (19) can be transformed as follows

$$\iint_S \left\{ \left(\rho_0 W + \frac{\rho}{\pi} \gamma_1\right) T''(t) + \left[\frac{\rho V}{2\pi}(\gamma_2 - \gamma_4) + 2\rho_0 \xi_0 W\right] T'(t) - \left(N_{0x} \frac{\partial^2 W}{\partial x^2} + N_{0y} \frac{\partial^2 W}{\partial y^2} + \frac{\rho V^2}{2\pi} \gamma_3\right) T(t) \right. \\ \left. - h \left(\frac{\partial^2 \Phi}{\partial y^2} \frac{\partial^2 W}{\partial x^2} + \frac{\partial^2 \Phi}{\partial x^2} \frac{\partial^2 W}{\partial y^2}\right) T^3(t) \right\} W(x,y) dx dy = 0 \tag{20}$$

Where the domain of integration S is $\{0 \leq x \leq a, 0 \leq y \leq b\}$.

Eq. (20) can be simplified as

$$AT''(t) + BT'(t) - CT(t) - DT^3(t) = 0 \tag{21}$$

where

$$\begin{aligned}
 A &= \iint_S \left(\rho_0 W + \frac{\rho}{\pi} \gamma_1 \right) W dx dy \\
 &= \rho_0 \iint_S \left(\sin \frac{m\pi x}{a} \sin \frac{n\pi y}{b} \right)^2 dx dy + \frac{\rho}{\pi} \iint_{Ra} \left(\iint_{Ra} \frac{1}{r} \sin \frac{m\pi \xi}{a} \sin \frac{n\pi \eta}{b} d\xi d\eta \right) \sin \frac{m\pi x}{a} \sin \frac{n\pi y}{b} dx dy \\
 &= \frac{\rho_0 ab}{4} + \frac{\rho}{\pi} \alpha_1 \\
 \alpha_1 &= \iint_S \left(\iint_{Ra} \frac{1}{r} \sin \frac{m\pi \xi}{a} \sin \frac{n\pi \eta}{b} d\xi d\eta \right) \sin \frac{m\pi x}{a} \sin \frac{n\pi y}{b} dx dy \\
 B &= \frac{\rho V}{2\pi} \iint_S (\gamma_2 - \gamma_4) W dx dy + 2\rho_0 \xi_0 \iint_S W^2 dx dy \\
 &= \frac{\rho m V}{2a} \iint_S \left(\iint_{Ra} \frac{1}{r} \cos \frac{m\pi \xi}{a} \sin \frac{n\pi \eta}{b} d\xi d\eta \right) \sin \frac{m\pi x}{a} \sin \frac{n\pi y}{b} dx dy \\
 &\quad - \frac{\rho V}{2\pi} \iint_S \left[\iint_{Ra} \frac{1}{r^3} (x - \xi) \sin \frac{m\pi \xi}{a} \sin \frac{n\pi \eta}{b} d\xi d\eta \right] \sin \frac{m\pi x}{a} \sin \frac{n\pi y}{b} dx dy \\
 &\quad + 2\rho_0 \xi_0 \iint_S \left(\sin \frac{m\pi x}{a} \sin \frac{n\pi y}{b} \right)^2 dx dy \\
 &= \frac{\rho m V}{2a} \alpha_2 - \frac{\rho V}{2\pi} \alpha_4 + \frac{\rho_0 \xi_0 ab}{2} \\
 \alpha_2 &= \iint_S \left(\iint_{Ra} \frac{1}{r} \cos \frac{m\pi \xi}{a} \sin \frac{n\pi \eta}{b} d\xi d\eta \right) \sin \frac{m\pi x}{a} \sin \frac{n\pi y}{b} dx dy \\
 \alpha_4 &= \iint_S \left[\iint_{Ra} \frac{1}{r^3} (x - \xi) \sin \frac{m\pi \xi}{a} \sin \frac{n\pi \eta}{b} d\xi d\eta \right] \sin \frac{m\pi x}{a} \sin \frac{n\pi y}{b} dx dy \\
 C &= \iint_S \left(N_{0x} \frac{\partial^2 W}{\partial x^2} + N_{0y} \frac{\partial^2 W}{\partial y^2} + \frac{\rho V^2}{2\pi} \gamma_3 \right) W dx dy \\
 &= \iint_S N_{0x} \frac{\partial^2 W}{\partial x^2} W dx dy + \iint_{Ra} N_{0y} \frac{\partial^2 W}{\partial y^2} W dx dy + \frac{\rho V^2}{2\pi} \iint_{Ra} \gamma_3 W dx dy \\
 &= -\frac{m^2 \pi^2 b N_{0x}}{4a} - \frac{n^2 \pi^2 a N_{0y}}{4b} + \frac{\rho m V^2}{2a} \alpha_3 \\
 \alpha_3 &= \iint_S \left(\iint_{Ra} \frac{1}{r^3} (x - \xi) \cos \frac{m\pi \xi}{a} \sin \frac{n\pi \eta}{b} d\xi d\eta \right) \sin \frac{m\pi x}{a} \sin \frac{n\pi y}{b} dx dy \\
 D &= \iint_S h \left(\frac{\partial^2 \Phi}{\partial y^2} \frac{\partial^2 W}{\partial x^2} + \frac{\partial^2 \Phi}{\partial x^2} \frac{\partial^2 W}{\partial y^2} \right) W dx dy \\
 &= -\frac{hm^2 n^2 \pi^4 (\alpha + \beta)}{2ab}
 \end{aligned}$$

$A \neq 0$ ($A \leq 0$ may occur only when $b/a \ll 0.1$, it wouldn't take place in actual projects), let $e = B/A$, $c = -C/A$, $d = -D/A$, Eq. (21) can be transformed into

$$T''(t) + eT'(t) + cT(t) + dT^3(t) = 0 \quad (22)$$

Obviously, Eq. (22) is a nonlinear differential equation with respect to $T(t)$, assume the periodic solution which satisfies the initial condition $T(t)|_{t=0} = 0$ is

$$T(t) = f \sin \omega t = f \sin \theta \quad (23)$$

where f denotes the amplitude.

Substituting Eq. (23) into Eq. (22), and applying the Bubnov-Galerkin method again yields

$$\begin{aligned} & \int_0^{T_0} (T'' + eT' + cT + dT^3) \sin \theta dt \\ &= \int_0^{T_0} (-f\omega^2 \sin \theta + ef\omega \cos \theta + cf \sin \theta + df^3 \sin^3 \theta) \sin \theta dt \\ &= -f \int_0^{T_0} (\omega^2 - c - \frac{3}{4}df^2) \sin^2 \theta dt + ef\omega \int_0^{T_0} \cos \theta \sin \theta dt - \frac{1}{4}df^3 \int_0^{T_0} \sin 3\theta \sin \theta dt = 0 \end{aligned} \quad (24)$$

where T_0 is a cycle.

Integrating and simplifying Eq. (24) yields

$$\omega^2 = c + \frac{3}{4}df^2 \quad (25)$$

When the wind velocity is reaching the critical value, the increasing aerodynamic will equal or even exceed the sum of deadweight and inertia force of the structure. Just at the moment, the frequency of the system characteristic equation becomes zero and the divergence instability phenomenon appears, just like the static equilibrium instability (Kornecki *et al.* 1976).

The critical condition for divergence instability is $\omega = 0$. Substituting A , C , D and $\omega = 0$ into Eq. (25) yields the critical divergence instability wind velocity

$$V_{cr} = \pi \sqrt{\frac{a(m^2 b N_{0x}/a + n^2 a N_{0y}/b)/2 + 3hm^2 n^2 \pi^2 f^2 (\alpha + \beta)/4b}{\rho m \alpha_3}} \quad (26)$$

From Eq. (25) we can conclude that in large amplitude theory the vibration frequency ω relates to the amplitude f , it is just one of the characteristics of geometric nonlinear structures. When f approaches zero, Eq. (26) can be transformed into the formula obtained just according to the small amplitude theory

$$V_{cr} = \pi \sqrt{\frac{a(m^2 b N_{0x}/a + n^2 a N_{0y}/b)}{2\rho m \alpha_3}} \quad (27)$$

4. Computational examples and discussion

Known from (25), the critical velocity V_{cr} is connected to the membrane parameters, structure sizes, pretension, orders and amplitude. We take the membrane material as an example which is applied in project commonly. $E_1 = 1400$ MPa, $E_2 = 900$ MPa, $\rho = 1.226$ kg/m³, $h = 0.001$ m, $a = 20$ m, $m = n = 1$, $f = 1$ m, $N_{0x} = 2$ kN/m. $\lambda = b/a$ denotes the span ratio of across-wind (y) to along-wind (x); $\gamma = N_{0x}/N_{0y}$ denotes the pretension ratio of direction x to y . The value of α_3 can be obtained by numerical integration method after all parameters are determined.

4.1 Span ratio λ

The curve of span ratio and critical wind velocity is shown in Fig. 2.

We can draw conclusions from the analysis of Fig. 2. With the increasing of span ratio λ , the critical wind velocity V_{cr} decreases gradually, when $0 < \lambda < 3$, it decreases sharply; when $\lambda > 3$, it decreases gently. It shows that the span ratio value should not be given too large in designing this kind of structure.

For the orthotropic characteristic, from the two conditions $E_1 > E_2$ and $E_1 < E_2$ we can conclude: when $\lambda < 1$, a greater V_{cr} value can be obtained if the small modulus is arranged to the along-wind

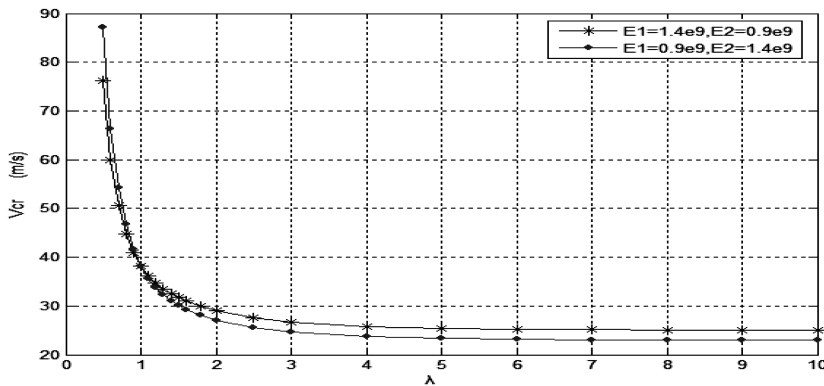


Fig. 2 Curve of span ratio λ and critical wind velocity V_{cr}

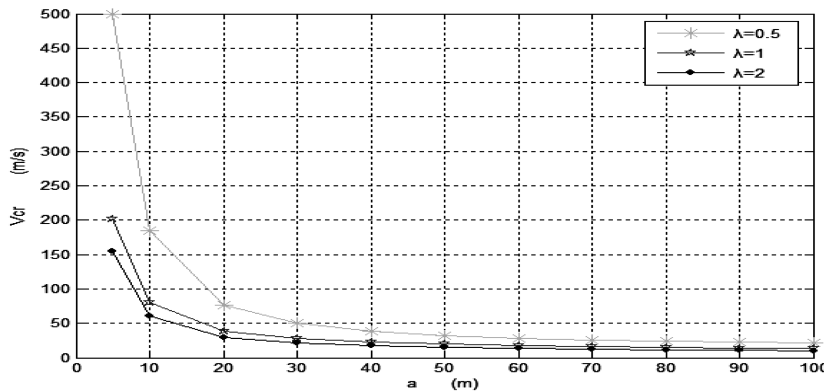


Fig. 3 Curve of along-wind span a and critical wind velocity V_{cr}

direction, the smaller λ is, a greater V_{cr} value can be obtained; when $\lambda > 1$, the situation is just right opposite; when $\lambda = 1$, tow V_{cr} values are equal.

4.2 Along-wind span a

The curve of along-wind span and critical wind velocity is shown in Fig. 3.

At different λ , with the increasing of span a the critical wind velocity V_{cr} decreases gradually, when $a < 20$ m, it decreases sharply; when $a > 20$ m, it decreases gently (see Fig. 3).

4.3 Pretension in x N_{0x}

The curve of pretension in x and critical wind velocity is shown in Fig. 4.

At different λ , with the increasing of pretension N_{0x} the critical wind velocity V_{cr} increases gradually, and all of them present weak non-linear in general (see Fig. 4).

4.4 Pretension ratio γ

The curve of pretension ratio and critical wind velocity is shown in Fig. 5.

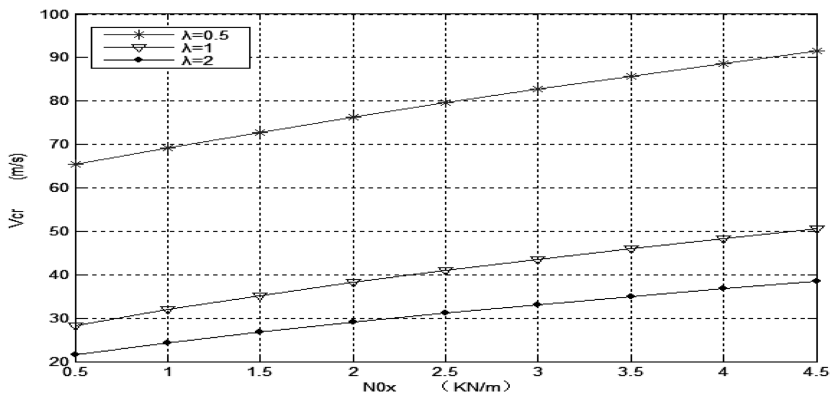


Fig. 4 Curve of pretension N_{0x} and critical wind velocity V_{cr}

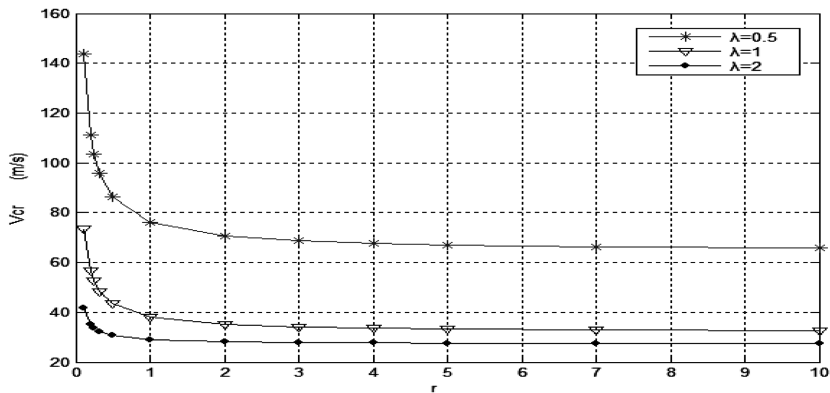


Fig. 5 Curve of pretension ratio γ and critical wind velocity V_{cr}

At different λ , with the increasing of pretension ratio γ the critical wind velocity V_{cr} decreases gradually, when $\gamma \leq 1$, it decreases sharply; when $\gamma > 1$, it decreases gently (see Fig. 5). Fig. 5 shows that, while along-wind pretension N_{0x} keeps constant and the across-wind pretension N_{0y} increases gradually, only when N_{0y} is greater than N_{0x} does the critical wind velocity V_{cr} increase sharply.

4.5 Amplitude f

The curve of amplitude and critical wind velocity is shown in Fig. 6.

With the increasing of amplitude f the critical wind velocity V_{cr} increases gradually, the smaller λ is, the more sharply V_{cr} increases. When $f \rightarrow 0$, V_{cr} is equal to the result obtained with small amplitude (see Fig. 6).

4.6 Orders in x and y m, n

The critical wind velocity in different orders is shown in Table 1.

When λ is small ($\lambda = 0.25$), the trend of divergence instability presents high orders instability in the along-wind x ($m > n = 1$). With λ increasing, the trend presents low order instability ($m = n = 1$). With the orders increasing, the critical wind velocity V_{cr} increases gradually in general. When $\lambda \leq 1$, the increase of across-wind order does more contribution to the critical wind velocity than the along-wind order does; when $\lambda > 1$, the situation is just right opposite (see Table 1).

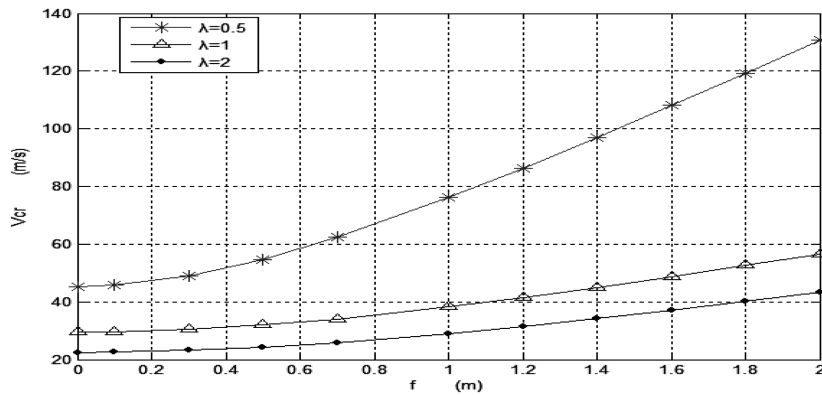


Fig. 6 Curve of amplitude f and critical wind velocity V_{cr}

Table 1 The critical wind velocity V_{cr} (m/s)

Order	$m = 1, n = 1$	$m = 2, n = 1$	$m = 3, n = 1$	$m = 1, n = 2$	$m = 1, n = 3$	$m = 2, n = 2$	$m = 3, n = 3$
$\lambda = 0.25$	256.48	179.41	162.08	1221.48	2904.69	853.99	1662.67
$\lambda = 0.5$	76.25	71.26	94.7	313.32	762.75	202.66	366.23
$\lambda = 1$	38.21	54.15	85.84	91.01	202.33	75.06	125.63
$\lambda = 2$	29.07	51.1	84.66	39.59	60.9	54.98	91.3
$\lambda = 4$	25.84	50.09	84.36	28.84	33.23	51.15	85.94

Derived from the above analysis of various parameters, the span ratio λ plays a more complex role than others in the aerodynamic stability of membrane structures, so it's the main control parameter in designing this kind of structure and needs to be paid sufficient attention.

5. Conclusions

We use the analytical method to analyze the aerodynamic stability of rectangular orthotropic membrane structures with large amplitude theory. The critical velocity formula obtained in this paper reflects the characteristics of orthotropic and geometric nonlinearity. The main analysis results are summarized as follows:

(a) With the influence of orthotropic in actual engineering, it has positive significance to arrange the membrane's warp and weft rationally according the local wind regime characteristics for preventing the instability destruction of structures.

(b) For the consideration of large amplitude, the stress in x and y directions will increase with the increase of deflection. The stress increment can improve the lateral rigidity and enhance the aerodynamic stability of the structure. The results more tally with the actual situation and more reasonable than the results calculated according to the small amplitude theory. We can determine a reference design value of amplitude f with an initial force (which is obtained by the local basic wind pressure) acting on the membrane.

From the discussion above we can see, the damping coefficient ξ_0 has no effect on the divergence instability wind velocity, and it's necessary to do some numerical analysis and experimental study about the rationality. The nonlinear governing equation and the critical wind velocity formula obtained in this paper have provided a theoretical foundation for the aerodynamic stability of the membrane structures. Based on the results given in this paper, the three-dimensional form of membrane structure will be studied in the author's following work, including necessary wind tunnel test when actual condition permits.

Acknowledgements

This work is supported by the Fundamental Research Funds for the Central Universities (Project Number: CDJZR10 20 00 10).

References

- Attar, P.J. and Dowell, E.H. (2005), "A reduced order system ID approach to the modeling of nonlinear structural behavior in aeroelasticity", *J. Fluid Struct.*, **21**, 531-542.
- Bingnan, S., Guodong, M. and Wenjuan, L. (2003), "Wind induced coupling dynamic response of closed membrane structures", *Proceeding of Eleventh International Conference on Wind Engineering*, Sanya, Hainan, December.
- Dowell, E.H. (1970), "Panel flutter: A review of the aeroelastic stability of panel and shells", *AIAA J.*, **8**(3), 385-399.
- Forsching, H.W. (1980), *Principles of Aeroelasticity*, Shanghai Science & Technology Press, Shanghai. (in Chinese)

- Ivovich, V.A. and Pokrovskii, L.N. (1991), *Dynamic Analysis of Suspended Roof Systems*, A.A. Balkema, Rotterdam.
- Kawakita, S., Bienkiewicz, B. and Cermak, J.E. (1992), "Aeroelastic model study of suspended cable roof", *J. Wind Eng. Ind. Aerod.*, **42**, 1459-1470.
- Kornecki, A., Dowell, E.H. and O'Brien, J. (1976), "On the aeroelastic instability of two-dimensional panels in uniform incompressible flow", *J. Sound Vib.*, **47**(2), 163-178.
- Li, Q.X. and Sun, B.N. (2006), "Wind-induced aerodynamic instability analysis of the closed membrane roofs", *J. Vib. Eng.*, **19**(3), 346-353.
- Minarni, H., Okuda, Y. and Kawamura, S. (1993), "Experimental studies on the flutter behavior of membranes in a wind tunnel", *Space Struct.*, **4**, 935-945.
- Miyake, A., Yoshimura, T. and Makino, M. (1992), "Aerodynamic instability of suspended roof modals", *J. Wind Eng. Ind. Aerod.*, **42**, 1471-1482.
- Scott, R.C., Bartels, R.E. and Kandil, O.A. (2007), "An aeroelastic analysis of a thin flexible membrane", *Proceedings of the 48th AIAA/ASME/ASCE/AHS/ASC Structures, Structural Dynamics, and Materials Conference*, Honolulu, Hawaii, April.
- Shin, C.H., Kim, W.S. and Chung, J.T. (2004), "Free in-plane vibration of an axially moving membrane", *J. Sound Vib.*, **272**(1-2), 137-154.
- Stanford, B., Ifju, P., Albertani, R. and Shyy, W. (2008), "Fixed membrane wings for micro air vehicles: Experimental characterization, numerical modeling, and tailoring", *Prog. Aerosp. Sci.*, **44**(4), 258-294.
- Stanford, B., Sytsma, M., Albertani, R., Viieru, D., Shyy, W. and Ifju, P. (2007), "Static aeroelastic model validation of membrane micro air vehicle wings", *AIAA J.*, **45**(12), 2828-2837.
- Sygulski, R. (1994), "Dynamic analysis of open membrane structures interaction with air", *Int. J. Numer. Meth. Eng.*, **37**(11), 1807-1823.
- Sygulski, R. (1997), "Numerical analysis of membrane stability in air flow", *J. Sound Vib.*, **201**(3), 281-292.
- Uematsu, Y. and Uchiyama, K. (1986), "Aeroelastic behavior of an H.P.shaped suspended roof", *Proceedings of the IASS Symposium on Membrane Structures and Space Frame*, Osaka, May.
- Yang, Q.S. and Liu, R.X. (2006), "Studies on aerodynamic stability of membrane structures", *Eng. Mech.*, **23**(9), 18-24.
- Zheng, Z.L., Liu, C.J., He, X.T. and Chen, S.L. (2009), "Free vibration analysis of rectangular Orthotropic Membranes in Large Deflection", *Math. Probl. Eng.*, Article ID 634362, doi:10.1155/2009/634362.